Journal of Computer Science

Original Research Paper

Dehazing Mechanism Using Auto-Encoder with Intensity Attention System

[1]Rajat Tiwari, [1,2]Bhawna Goyal and [3]Ayush Dogra

[1]*Department of Electronics and Communication Engineering, Chandigarh University, Mohali, India*
[2]*Faculty of Engineering, Sohar University, Sohar, Oman*
[3]*Chitkara University Institute of Engineering and Technology, Chitkara University, Punjab, India*

Article history
Received: 29-06-2024
Revised: 17-08-2024
Accepted: 30-08-2024

Corresponding Author:
Rajat Tiwari
Department of Electronics and Communication Engineering, Chandigarh University, Mohali, India
Email: er.rajattiwari@gmail.com

Abstract: In the modern world, images play a significant medium for communication. Primarily, it is easily transferred and disseminated across various platforms which allows the people to express their ideology and perceptions. Conversely, images can be prone the environmental conditions as the image quality can be affected by the weather circumstances. Particularly, haze images minimize the whole clarity and visibility of the image. It is necessary to dehazed the image to retain the image quality and enhance the clarity of the image. Conventionally, the manual dehazing method includes altering several parameters and utilization of image editing software. It is a time-consuming mechanism, less efficient, and can be prone to manual error. To resolve the issue, traditional researchers utilized various techniques for the dehazing mechanism but lacked accuracy and speed. To address the issue, the proposed research employs an encoder that uses focus flex and entropy fade component blocks with an attention mechanism for the dehazing model. Moreover, the attention mechanism is used to highlight substantial data to enhance accuracy. Correspondingly, dense-haze and FRIDA datasets are used for the dehazing function to augment the efficiency. Accordingly, the respective model is evaluated with the performance metrics to examine its efficiency. Furthermore, comparative analysis is carried out to reveal the presented research's greater performance.

Keywords: Autoencoder, Attention Mechanism, Deep Learning, Focus Flex, Entropy Fade Component Blocks

Introduction

In recent times, the image includes varied nature, dimension, and hazy smog that can reduce the image quality and it is significant to achieve the spatial framework, and progressive development, with the spectral configuration of the object to understand the natural phenomena in the better way (Yang *et al*., 2020). Besides, image restoration transferences a stimulating work to progress the image, specifically in the area of therapeutic imaging, digital cinematography, video surveillance, and so on (Mi *et al*., 2020). Further, the images taken from the outdoors are frequently corrupted through haze, an atmospheric phenomenon formed by minor floating elements that engross and sprinkle the light after proliferation direction. Moreover, haze influences the reflectivity of such section as it produces contrast loss on the distant objects, discerning reduction of the light range, with added noise. Hence, reinstating such images remains vital in numerous open-air implementations namely, photographic observation and automated driving assistance. Formerly, the methods depend on atmospheric indications, and on several imageries taken with separation filters (Ancuti *et al*., 2018).

Many single-image dehazing methods have been presented in an effort to improve the visibility of hazy imageries and few have attained substantial growth. Normally, haze deduction procedures can be classified into two models, namely, classical and Deep Learning (DL) based approaches (Tran *et al*., 2022). Moreover, the DCP technique is the most conventional dehazing procedure acquired from arithmetical preceding information. On the other hand, it typically renounces after the circumstantial light intensity remains high. To solve the limitations of the DCP method, the guided filter dehazing algorithm has been proposed. As, the haze noise is typically categorized in huge ascent with small variance in entire directions focused on it, the directed filter de-

hazing algorithm detects the haze region remains independent of the circumstantial light. Though an extensive number of preceding information has been incorporated into traditional dehazing procedures to advance efficacy, the procedures lead to the problem of inadequate strength (Zhao *et al*., 2021). Through the upsurge of DL, various approaches were initiated to use Neural Networks (NN) to evaluate unidentified factors in typical models. However, the valuation accuracy of unidentified factors disturbs the dehazed imageries quality (Dong *et al*., 2020). Consequently, several approaches initiate to dehazed images with DL models. End-to-end DL methods directly regress haze-free images from hazy images, deprived of relying on defective substantial models factor valuation, attaining better dehazing efficiency. However, the dehazing supporting system of the approaches (Pan *et al*., 2021) utilizes a normal encoder-decoder framework (Meng *et al*., 2022). On the other hand, a common distinctive in aerial imageries and ground-level imageries with the occurrence of haze effects remain with lesser dissimilarity and pale colors, creating additional handling of the imageries for detecting the object and classification are challenging.

To resolve the limitation of the conventional model, the proposed system used Focus Flex and Entropy Fade Component Auto-encoder with an Intensity Attention System. Initially, hazed image datasets such as dense haze and FRIDA images are loaded into the pre-processing unit. The input image datasets are trained and split. The images are auto-encoded with Focus Flex and Entropy Fade Component block. The features acquired from the model are fused by using the dot-product method. The attention mechanism is used to highlight the significant features. Besides, the predicted test images are obtained and the performance metrics are calculated. Finally, the dehazed image is acquired as the output.

The main contribution of the proposed method is as follows:

- To employ auto-encoder of focus flex and entropy block with attention mechanism using dense haze and FRIDA dataset for dehazing mechanism to enhance the efficiency in the proposed system
- To apply features fusion with dot product in improving dehazing performance
- To use performance metrics to calculate the respective research efficiency

Literature Review

Natural imageries that are captured in haze weather have difficulties with lesser contrast and color saturation with high intensity. Haze imageries as input can extensively upsurge the difficulty in handling radical images. Consequently, dehazing such imageries remains a significant stage formerly executing unconventional images (Meng *et al*., 2022).

Accordingly, classical dehazing procedures have achieved image dehazing by increasing image intensity and contrast or creating synthetic priors like color reduction priors with dark-channel priors. However, the result is unbalanced when allocating difficult sights (Meng *et al*., 2022). Hence, the existing structure centered on PDR-Net used a hierarchal distended convolution with pre-processing elements, treating units, and post-processing parts, with attention implementations. The existing network is trained to minimize L-1 and perceptual loss using the O-Haze dataset. Then the result can be evaluated by using Structural Similarity Index Measure (SSIM), Peak Signal-to-Noise Ratio (PSNR) that has utilized the O-Haze dataset by SSIM (0.798), a PSNR (25.39) and not enhanced with a color variation (Hartanto and Rahadianti, 2021). Moreover, a prevailing DCPDN remains as an end-to-end mutually optimizable dehazing network framed by implanting a model directly into the optimization structure through arithmetic processing elements. Accordingly, the method permits the network to enhance the transmission diagram, atmospheric light, and dehazed image equally. The GFN remains a fusion-based dehazing technique and produces visually fair outcomes for maximum circumstances. Conversely, the GFN cannot manage hazy imageries of outsized haze regions. Additionally, the dehazing capability of the GFN is restricted through its sources after the inputs, which are supposed to comprise flawless signs to rebuild the dehazed image (Zhang and He, 2020).

On the other hand, a classical squeeze-and-excitation block, FCA utilizes the low-frequency spectrogram to achieve the attention weight coefficient in the frequency domain, generating it by training that focused on the image at low-frequency region. General evaluation tests verify that the existing KFA-Net has a great advantage. PSNR and SSIM of KFA-Net are 31.0952 and 6.6401% greater than DCP respectively (Jiang *et al*., 2023). The prevailing method has utilized the visual possessions of hazy imageries and incorporates three haze-related structures into a linear method for transmission valuation, monitored through a learning method for resolving the indefinite constants. Moreover, the pixel-wise method needs no additional modification and avoids the failure circumstances of the prior-based approaches. However, the existing method has limitations when using the atmospheric sprinkle method. But it cannot have the ability to manage the dense haze with difficult scenarios (Wang *et al*., 2021). Besides, the Deep Guided Transformer Dehazing Network (DGTDN) method depends on the transformer with a channeled filter that increases the speed and the results with the quality of the dehazed image. To address the dehazing speed problem, the guided filter model is employed to perform a joint up-sampling. Hence, the dehazing speed and the quality of the dehazed image showed a better result (Wu *et al*., 2020).

In the existing method, the adaptive histogram equalization technique has been utilized as the data reliability element, the fractional derivative has been implemented to avoid over-development with noise magnification; and the prevailed data-driven regularization positions are implemented to extract the non-local and local structures of an image. Formerly, to resolve the problem, half-quadratic splitting is utilized. Furthermore, a dual-stream network centered on a Convolutional Neural Network (CNN) with a Transformer is presented to construct the data-driven regularization. As a result, the atmospheric covering has attained a better outcome (Jiao *et al*., 2022). Moreover, the Atmospheric Light Scattering (ALS) method has two unknowns such as atmospheric light and transmission map that are projected against the section. Besides, a preceding method is engaged for dehazing the images in the mobile devices along the comparison is done on a number of rotations at the pre-specified threshold. Moreover, if the amount of rotation is less means, the section can utilize the pre-estimated atmospheric light. Hence, the existing method need not to re-evaluated at each time and the overall dehazing process showed better results (Cimtay, 2021).

The End-To-End Adaptive Enhancement Dehazing Network (AED-Net) technique is used to recover flawless sections after hazy imageries. Besides, the Codalab NTIRE 2021 dataset is used to evaluate the method quantitatively and qualitatively. Hence, wide-ranging computer simulations proved that AED-Net has shown a better result with regard to PSNR, SSIM also with further key metrics (Hovhannisyan *et al*., 2022). Similarly, the existing SRD process on a huge amount of real-time and synthetic haze RSIs is compared with the former methods. When the SRD algorithm has exposed an enhancement in usual color fidelity, distinct structural contours and overall visual quality are improved. Besides, the quantitative assessment depends on full-reference and no-reference IQAs to determine that SRD has better dehazing efficiency (He *et al*., 2023).

As various determinations of imageries, the intentions of blocks convoluted in the existing study are accomplished through adaptive techniques. Correspondingly, the existing method associated with the adaptive threshold reduction technique is utilized for low-rank with sparse decomposition. Consequently, the granular approximation of the atmospheric covering has been achieved by a guided filter with an adaptive radius for refinement with the accurate atmospheric light with the openly accessible datasets demonstrated by the dehazed imageries (Bi *et al*., 2022). Moreover, the existing model is suitable for blind Gaussian de-noising in a learning structure at hidden layers. By means of existing complexity maps, the images with greater quality have been obtained by inverse sprinkled image generation method and achieve de-haze images. The existing algorithm has been performed and it is compared with 16 advanced techniques on the Ground Truth (GT) O-Haze dataset and it has shown a better performance (Roy, 2022).

Problem Identification

There are certain limitations which are identified in the implementation of the existing methods that are represented below:

- The particularly dense and irregularly circulated haze in the test sample, can cause certain irreparable loss of image data and reduce the Solid-state Reflective Display (SRD) process ineffective for hazy image restoration (He *et al*., 2023)
- Several conventional models used a single dataset for the dehazing mechanism. Conversely, the utilization of diverse datasets in a single system is lacking in the existing research (Jiao *et al*., 2022)

Materials and Methods

Environmental configuration of the obtaining the results for the proposed model is tabulated in Table (1), where hardware and software configurations used for implementing the results of the model is listed.

Photography in foggy weather frequently leads to poor quality, blurring, and diverse images. However, it is a challenging task to remove the haze in the image to enhance the quality. Several conventional techniques have been developed, but they have some complications in attaining high accuracy along with computation speed. Hence, the propounded model has employed Focus Flex Block and Entropy Fade Component Block with Attention Block method for image dehazed through the reside dataset, where the hazed images are converted into de-hazed images by using the proposed model.

Figure (1) represents the overall flow of the proposed model. It is identified that the proposed system comprises the following techniques:

- Data selection
- Pre-processing
- Image enhancing mechanism
- Performance metrics

Table 1: Environmental configuration

Hardware-configuration	Software tools
CPU-Intel Core i7-7700@2.80 GHz	Windows 10
GPU - GTX 1050	Python-3.7
RAM: 16 GB	Anaconda-Spyder

DOI: 10.3844/jcssp.2024.1805.1817

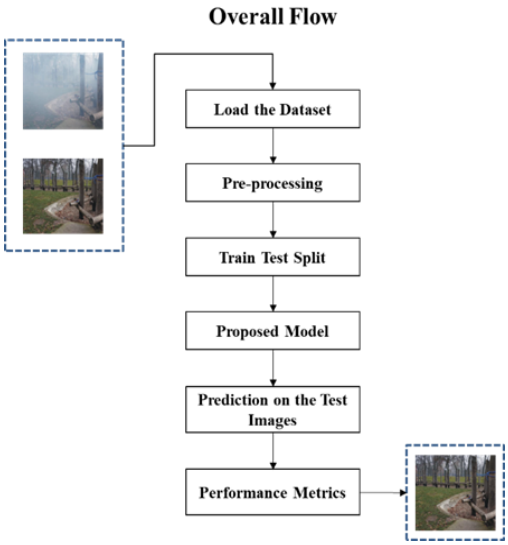

Fig. 1: Overall flow of the proposed model

Correspondingly, a detailed depiction of the respective model is signified in the following subsections.

Data Selection

This section represents the selection of data utilized for the proposed method. The data are selected from dense-haze and FRIDA.

Dense-Haze Dataset

Whereas, the dense haze comprises 33 pairs of real hazy and equivalent haze-free imageries of numerous outside sights. Besides, the hazy and haze-free sights comprise the similar visual content taken in the similar radiance factors. The dense-Haze dataset aims to push significantly the state-of-the-art in single-image dehazing by promoting robust methods for real and various hazy scenes.

FRIDA Dataset

Similarly, the FRIDA and FRIDA2 are databases of arithmetical imageries that are certainly functional to estimate in a methodical technique, where the efficiency of reflectivity with contrast restoration procedures. Besides, the FRIDA includes 90 artificial imageries of eighteen urban road sights.

Pre Processing

The purpose of the pre-processing is to ensure image re-sizing and format, assisting in model preparation and extrapolation. Moreover, resizing confirms that images adapt towards the normal dimensions, enabling batch processing also assist in sustaining a reliable aspect ratio through images.

Data Splitting

The complete data that is pre-processed and sent for the feature section sing optimal algorithms are divided in terms of train and the test data respectively. The initial, training data are used in training the model. Whereas, the latent, test data are used in the model validation or in testing the respective model. The data is split in the ratios of 80:20 for train and test data respectively.

Dehazing Mechanism

In Fig. (2) the framework of the proposed method is described where the haze and haze-free images are fed into the encoder. In the encoder block, all the images are studied layer by layer, which includes size, color, and so on. Further, it processes the hazy image to extract feature representations. This alteration captures vital information from the image when reducing its dimensionality.

Moreover, the Focus flex block helps adaptively enhance features and fuse information to produce high-quality de-hazed outcomes. The entropy is used to evaluate image texture whereas the fade indicator measures the ability to remove haze from images. Combining entropy with fading blocks can intend the information content and the fading regions to improve de-hazing performance. The features fusion block integrates corresponding information from both blocks and ensures a completely improved feature set. The attention mechanism selects focusing on de-hazing regions while maintaining overall brightness, leading to enriched de-hazing images. Finally, the de-haze image is up-sampled in the decoder and the de-hazed image is obtained as the result.

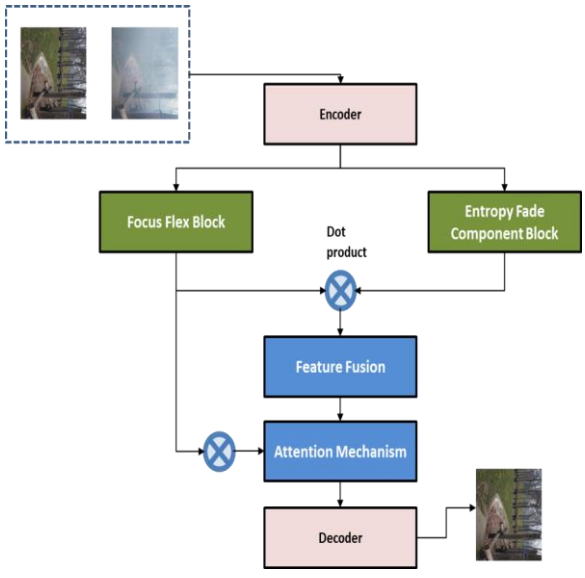

Fig. 2: Framework of proposed method

Focus Flex Block

The Focus Flex Block dynamically regulates the focus on significant features of the image. Moreover, "Focus Flex" is termed and is flexible, arranged at various parts of the image depending on the significance of de-hazing. It can include an adaptive mechanism, which signifies and improves foremost features such as boundaries and textures are essential for flawless visibility. The process of taking input images is given in the Eq. (1):

$$IN\ (i) = J\ (i)\ tras\ (i)\ +\ \alpha\ (1\ -\ tras\ (i) \tag{1}$$

where, *IN*(*i*) is the hazy image, *J*(*i*) represents the output image after feature maps restoration, *tras*(*i*)) is the medium transmittance α is the global atmospheric light intensity coefficient and I signify the index panel of the amplifying image. Furthermore, the haze image feature map regulates various concentrations by calculating α and β parameters. The *tras*(*i*) is simulated by computing the β and depth value to conclude the de-hazing result:

$$tras\ (i) =\ e^{-\beta d(i)} \tag{2}$$

where, β denotes the atmospheric scattering coefficient and *d*(*i*) represents the distance between the camera and the object.

Moreover, the haze removal parameters need precise estimation of α and *tras*(*i*) calculation for active de-hazing. The constant '*b*' is added in Eq. (4) in the parameters determination:

$$J\ (i) = 1/(tras\ (i)\ )(IN\ (i)\ -\ \alpha)\ +\ \alpha \tag{3}$$

Here, *J*(*i*) depicts the concatenation of the parameter. Similarly, Eqs. (4-7) represents the combination of the parameters conversion.

$$J(i) = 1/(\text{tras (i)}\ )\ (\text{IN (i)}\ -\ \alpha)\ +\ (\alpha\ -\ \text{b})\ +\ \text{b} \tag{4}$$

$$J(i) =\ [\text{IN (i)} -\ 1]\left[\frac{\frac{1}{\text{tras(i)}}((\text{IN (i)} - \alpha) + (\alpha - \text{b}))}{(\text{IN (i)} - 1)}\right] +\ \text{b} \tag{5}$$

$$J(i) =\ \text{K (i)}\ (\text{IN (i)}\ -\ 1)\ +\ \text{b} \tag{6}$$

Whereas:

$$K(i) =\ (\ 1/\text{tras(i)}\ ((\text{IN (i)} -\ \alpha) +\ (\alpha\ -\ \text{b})))/(\text{IN (i)} -\ 1) \tag{7}$$

Equation (6) expresses the incorporation of an exclusive parameter *K*(*i*) transformation and procedure, the de-hazing structure desires to predict one parameter to determine the hazy image, and the convolution computation is expressed.

Additionally, the multiple 1×1 convolution operations and Exponential Linear Unit (ELU) function extract smooth intensity feature maps. The ELUs contain negative values that drive mean unit activations nearer to zero, similar to batch normalization with less computing cost.

Correspondingly, *the ELU* function is mentioned in Eq. (8):

$$ELU(x) = \begin{cases} x, x\ >\ 0 \\ \alpha(e\ x\ -\ 1), x\ <\ 0 \end{cases} \tag{8}$$

The method of up-sampling images associated with feature maps, to prevent the initialization value from impacting the training procedure. The convolution magnifies *W* and *H* values by r times of each, and the data of *W*×*H*×(*C*×*r*^*2*) rearrange into data of *r*×*W*×*r*×*H*×*C*. To calculate the up-sampling output by using the Eq. (9):

$$\begin{aligned} &Input{:}\ IN^{LR}_{W\times H\times(C\times r\ 2)} \\ &Output{:}\ IN^{LR}_{r\times W\times r\times H\times C} \\ &IN^{SR}_{w,h,c^{\wedge}}\ =\ IN^{LR}_{p} \end{aligned} \tag{9}$$

Correspondingly, low-resolution images are depicted as I^{LR} width is mentioned as *W*, and height is shown as *H* of the I^{LR} feature map. The output I^{SR} denotes the high-resolution images and *C* remains as the number of channels of I^{LR}. Moreover, the variable r is the required magnification to amplify I^{LR} to I^{SR}.
where as:

$$p = \left\lfloor\frac{w}{r}\right\rfloor, \left\lfloor\frac{w}{r}\right\rfloor, C.mod(h,r) + C.mod(w.r) + \hat{c} \tag{10}$$

Here, variables *w*, *h*, and $\hat{c}$ are the width position, height, position, and channel number of current I^{SR} feature maps.

Entropy Fade Component Block

The entropy fade component block reduces the randomness in the feature representation. Further, the entropy fade proposes that the procedure selectively reduces noise and irrelevant variants in the image. This can include enhanced filtering methods or else reduction of noise using techniques that refine the haze when preserving significant details.

The degradation function *Ent* on training phase which evaluates the effects to be detached on the output imageries. Besides, the connection between the input image and the degraded image can be quantified as a loss function (*L*).

During the procedure of training, the over-degraded image IN* is the output image and it is related to the input image with *IN*. In, the entropy fade block it is assumed that $\theta = (w, b)$ where w remains as the weight matrix and b is denoted as the bias vector, the parameter of focus flex component block and $\hat{\theta} = (\hat{w}, \hat{b})$ is the parameters of entropy fade block. The hypothesis establishes that:

$$IN\ *=\ Ent(\hat{}I) \tag{11}$$

and:

$$\theta, \hat{\theta} = argmin\left[L\left(I, \hat{I}^{*}\right)\right] \quad (12)$$

Where I am the input image and $\hat{I}^{*}$ is the over-gradated output image.

Thus, reducing the variance among *IN* and *IN*' lets the image at decoder output be reinstated form of the input image (*IN*'):

$$\mathrm{IN}' = \mathrm{Ent} - 1\ (\mathrm{IN}) \quad (13)$$

The Loss Function is defined by adopting the Mean Square Error (MSE) value and then *L* is tested evaluated and specified in Eq. (14), where *IN* and *IN*" are represented as input and output images:

$$L = \frac{1}{N}\sum_{In=1}^{N}(IN - IN^{*})^{2} \quad (14)$$

In Eq. (15) where γ remains as the gamma factor, *A* is a constant (gain) its value is 1 and IN_s is the input from the dataset. Hence, the block is signified through the gamma correction. Whereas the loss block denotes the Eq. (14) and it is depicted in Eq. (15):

$$Ent = A.IN_{s}^{\gamma} \quad (15)$$

where, *Ent* is the degradation step over the training stage.

Feature Fusion

Feature Fusion is a technique for integrating the various extracted features against several databases to achieve a single feature file. The foremost objective of fusion methodology in de-hazing the images is to combine the discriminative and reliable data of completely derived features within individual vectors to enhance efficacy while decreasing the execution time of the system. The main objective of feature fusion is to decrease the feature size with noise removal. It can also syndicate two or more characteristics of various fields and eliminate the dimensionality curse problem with an increase in classification accuracy. Here, the extracted mages from the focus flex and entropy fade blocks are combined together in the feature fusion block. Where the de-hazed images with the better resolution are obtained and it is sent to the attention mechanism block to enhance the image features. The mapping of the Focus Flex block and Entropy Fade Component block function is given in Eq. (16).

$$Feat\_t = aW * concat(IN\_p^{LR}, Ent) + b \quad (16)$$

In Eq. (16), *W* denotes the weight and b represents the bias factors and eventually is defined as the stimulation function. IN_p^{LR} and *Ent* denote adjacent features and concat is a function that concatenates IN_p^{LR} *and Ent.*

Attention Mechanism

The attention mechanism procedures the fused features towards selectively highlight the utmost significant measures for de-hazing. They are intended to consider various measures of the feature map rendering towards the prominence, concentrating computational resources on the furthermost acute areas. This supports efficiently re-establishing brightness in the hazy area while sustaining the complete structure with information about the image.

The score of the initial phase is regularised and the softmax function is utilized to change the attention score as exposed in Eq. (17):

$$att_t = \frac{exp\ (Feat^{T}{}_{t}\ v)}{\sum exp\ (Feat_{t}^{T}\ v)'} \quad (17)$$

where, *v* remains as the attention value. $Feat_t^T$ shows the similarity or correlation between the output feature and the input feature. Whereas att_t is the attention mechanism calculation.

Finally, the decoder proceeds the attended with fused features also restructures the absolute de-hazed image. It converts the lower-dimensional features retained into a high-dimensional image, preferably with de-haze and better visibility and it is computed by Eq. (18):

As stated by the weight coefficient, the attention value is acquired through weighted calculation of value as exposed in Eq. (18):

$$sim = \sum_{t} att_t \quad (18)$$

where, t_t is the input vector. The hypothesis establishes the function of the decoder and it is expressed below:

$$Sim^{*} = Deg\ (\widehat{sim}) \quad (19)$$

And loss function is given by:

$$\widehat{sim}^{*} = \mathrm{A}.sim^{\gamma} \quad (20)$$

The overdegradated image $\widehat{sim}^{*}$ is the output image. A is the degradation step. In the attention mechanism, the entropy fades component block and the focus flex block are combined together giving the dehazed output. Where the product of *A* and sim^{γ} gives the value of $\widehat{sim}^{*}$.

Figure (3) illustrates the architecture of the respective system. In this mechanism, the image de-hazing is divided into two sections namely, an encoder that aims to extract significant features to de-haze hazy regions, whereas the decoder aims to restructure the de-hazed images by down-sampled images received from the encoder. Besides, in the proposed model, an input hazed image is encoded to extract the respective features. Where the encoded features are treated through the focus flex block to improve main features and the entropy fade component block is used to minimize noise and haze. The outputs from these blocks are fused to make a complete feature set. Moreover, the usage of an attention mechanism in this model selectively highlights the significant features for de-hazing, confirming that the restored image has greater clarity with features.

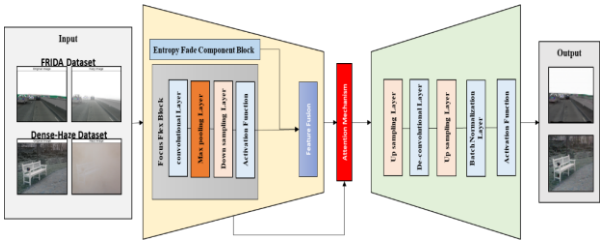

Fig. 3: Architecture of proposed method

Results and Discussion

This section mainly focuses on the result and discussion where, the EDA, performance metrics, performance analysis, experimental results, and comparative analysis are discussed in detail.

Exploratory Data Analysis (EDA)

EDA is used to analyze the entire dataset besides formal modeling and summarizes the main characteristics and key insights dataset. Figure (4) signifies the input image of the propounded system.

Figure (4) depicts an image from a dense haze dataset with hazed features. Further, the dataset comprises dense and homogenous hazy images, which means that the haze is evenly scattered over the images. The features permit a regulated atmosphere to calculate the de-hazing algorithm effectively. Moreover, the dataset contains 33 pairs of real haze images along with the equivalent de-hazing descriptions. Similarly, it contains various outdoor scenes, that are mostly affected by haze in real-world environments.

Figure (5) depicts an image from a dense FRIDA dataset with hazed features. Moreover, it contains the dense FRIDA and FRIDA2 subsets are designed to estimate visibility with contrast restoration procedures in foggy images. The fog images have features such as fog simulation, and depth maps which provide the facts of spatial configurations of objects in the images. Also, it shows visual characteristics such as color saturation, and minimized contrast with unclear overview of objects.

Performance Metrics

To predict the efficacy of restoration by calculating the quality of the image with parameters such as PSNR and SSIM.

Peak Signal to Noise Ratio (PSNR)

PSNR is in the calculation of the ratio between the maximum possible signal power and the power of the distorting noise which is a vital attribute that disturbs the quality. This is calculated using Eq. (21):

$$PSNR = 10\,log_{10}\frac{R^2}{MSE} \tag{21}$$

Here the R represents the distance among the points occurring in noise.

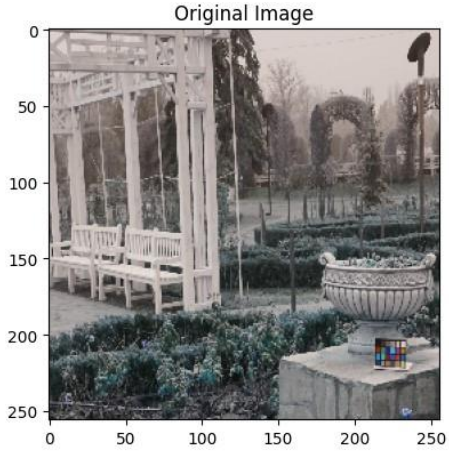

Fig. (4): Illustration of haze dataset image

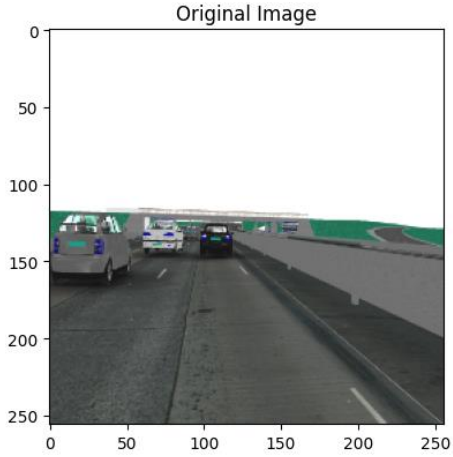

Fig. 5: Sample of the image from the Frida dataset

Structure Similarity Index Method (SSIM)

SSIM is a perception-based model. In this method, image degradation which is due to image compression techniques, or degradation can be due to a loss occurring during data transmission. Values closer to 1 represent better quality of the image. This is calculated using the Eq. (22):

$$SSIM\ (x,y) = \frac{(2\mu_x\mu_y+C_1)+(2\sigma_{xy}+C_2)}{\mu_x^2+\mu_y^2+C_1)(\sigma_x^2+\sigma_y^2+c_2)} \tag{22}$$

Here μ_x represents the average of x, μ_y represents an average of y, μ_x^2 Represents the variance of x, μ_y^2 represents the variance of y and σ_{xy} is the co-variance of x and y.

Experimental Results

Experimental results of the proposed study are discussed in this section.

Table (1) deliberates the performance metrics of FRIDA and the dense dataset. For PSNR, it shows 25.47 of dense haze, 30.27 of Frida-k 31.97 for Frida-I, 33.94 for Frida-m, and 31.81 for Frida-n. Likewise, it achieved better results for SSIM and Average gradient respectively.

Performance Analysis

The section explains the performance of dense haze and FRIDA datasets and it is expressed as follows. Fig. (6) represents the original images (Left Image) which functioned in the presented model (Middle image). The right image signifies the resulting de-hazed image. The right image signifies the resulting de-hazed image. From Fig. (6) it is inferred that the increase in the number of epochs mitigates the haze in the images, which results in the de-haze images. The right image signifies the resulting de-hazed image. Fig. (7) illustrates de-images at the FRIDA dataset of (k, l, m, n) and it showed de-hazed images at 1000 epochs.

Figure (8) represents the dense haze dataset loss plot for 200,500,800 and 1000 epochs and loss over function. It shows that the loss functions are lost at 1000 intensity. Similarly, Fig. (7) describes the epochs and loss representation of the FRIDA dataset.

Figure (9) describes the epochs and loss representation of the FRIDA dataset of 200 insentity of FRIDA (k, l, m, n) intensity. Table (2) shows a comparative analysis of PSNR and SSIM of the prevailing methods and the proposed method for the haze dataset, where the proposed method has acquired a PSNR value of 25.47 and SSIM of 0.8028.

Table 2: Performance metrics of dense and FRIDA dataset

Performance metrics	Dense haze	FRIDA-k	FRIDA-l	FRIDA-m	FRIDA-n
PSNR	25.4700	30.2700	31.9700	33.9400	31.8100
SSIM	0.8028	0.9376	0.9507	0.9636	0.9573
Avg_gradient	0.0305	0.0159	0.0159	0.0159	0.0160

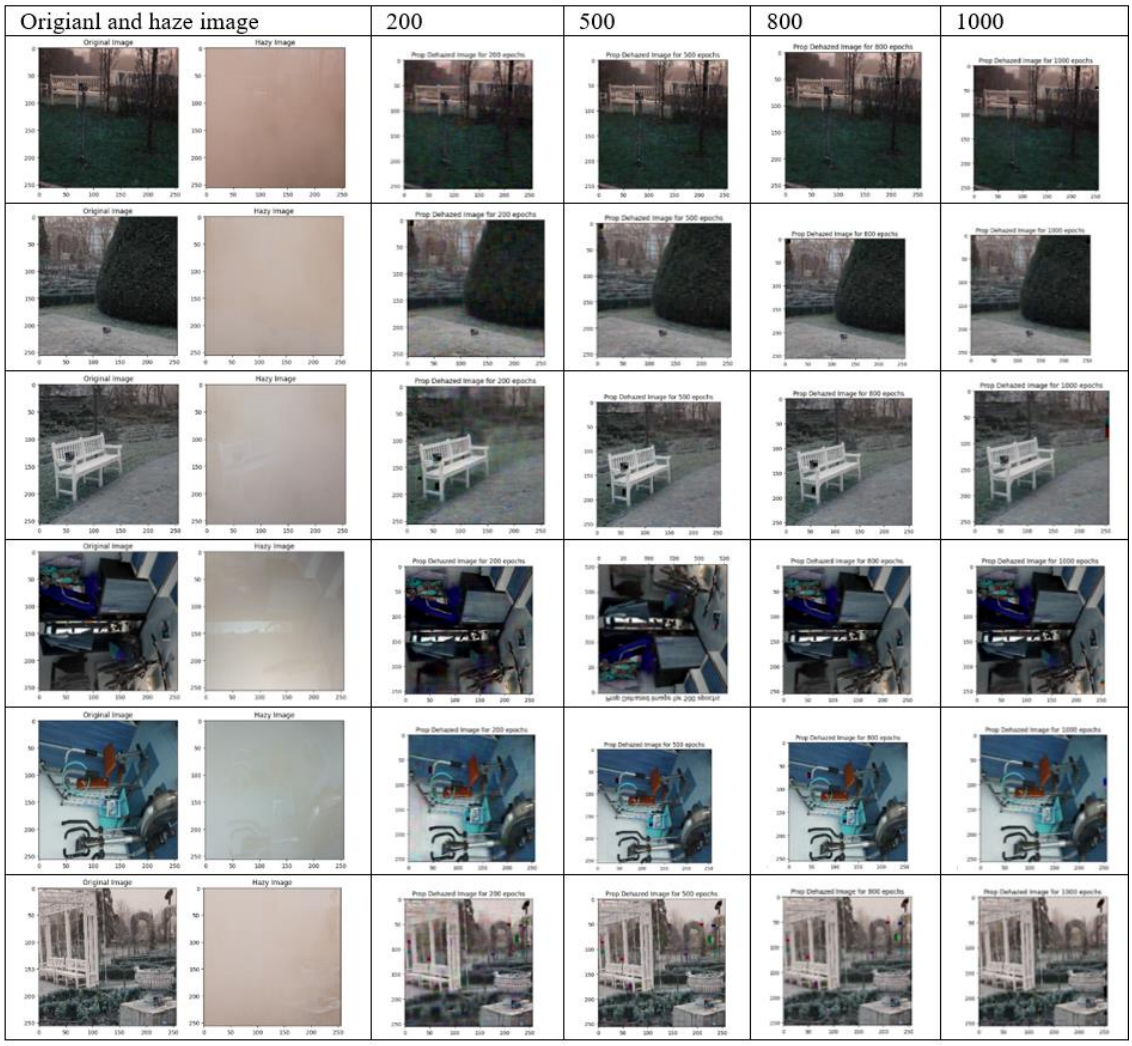

Fig. 6: Images of dense haze dataset

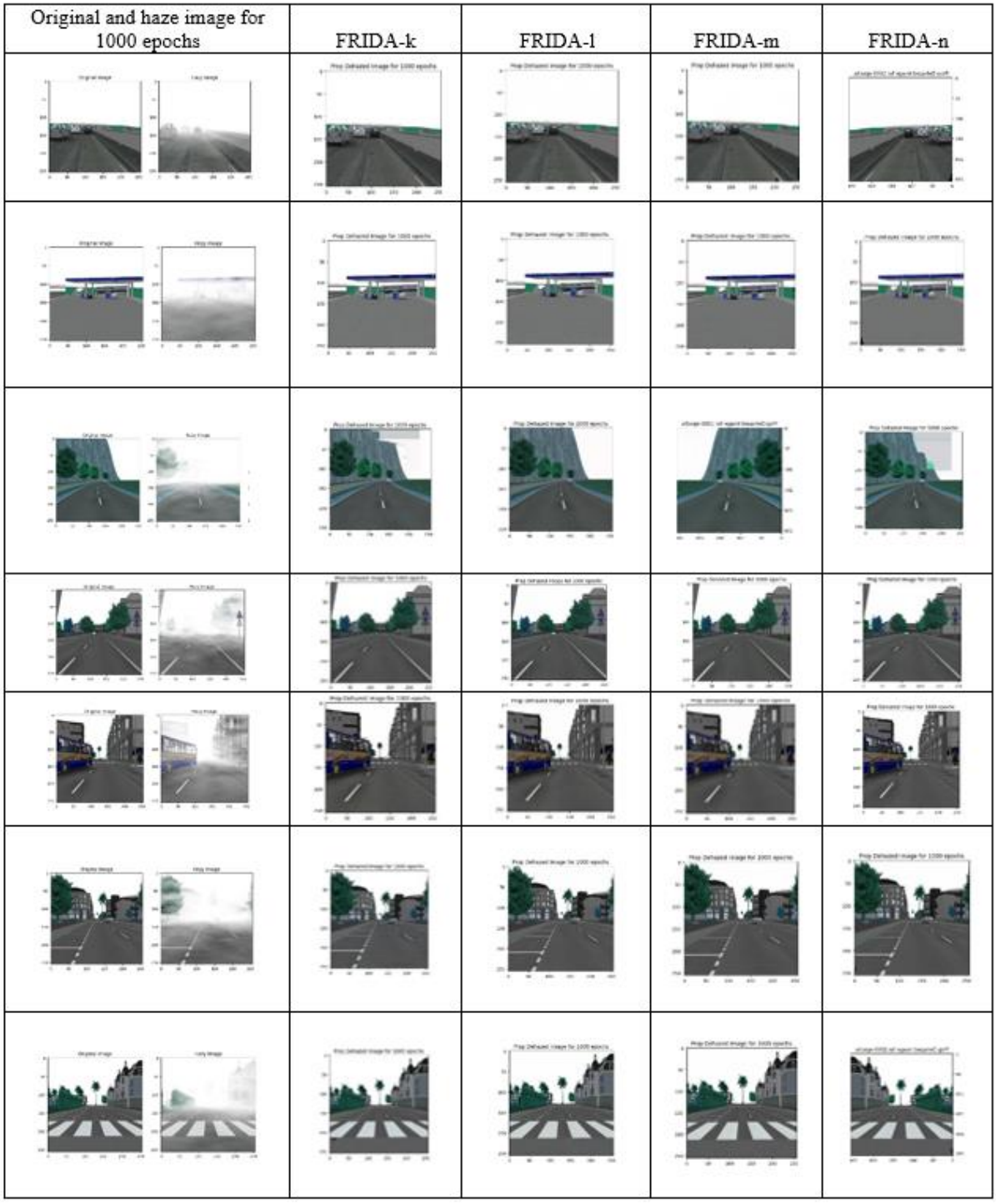

Fig.7. Images of FRIDA dataset

From the table, it is inferred that the proposed model has attained greater results when compared with the existing model. Where it has attained a PSNR value of 25.47 which is greater than the existing model. Similarly, the SSIM value is 0.8028 for the proposed model.

Comparison Analysis

The comparative analysis describes the comparison of PSNR and SSIM of the prevailing model and the proposed model.

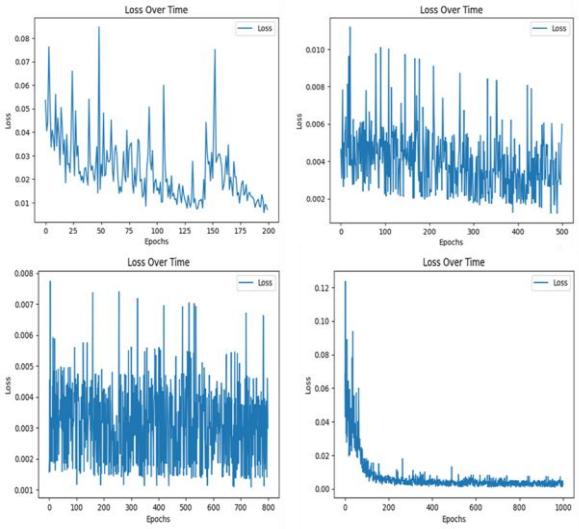

Fig. 8: Results of dense haze dataset

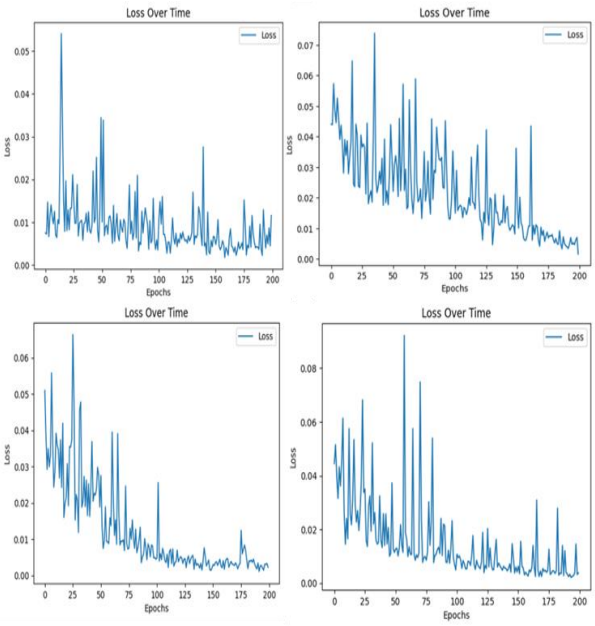

Fig. 9: Graphical representation of epochs and loss of Frida dataset

Table 3: Comparative analysis of haze dataset (Ancuti *et al*., 2018)

Model	PSNR	SSIM
Roy (2022)	16.586	0.735
Meng *et al*. (2013)	17.443	0.753
Fattal (Cimtay, 2021)	15.639	0.707
Meng *et al*. (2022)	16.207	0.666
Ancuti *et al*. (2018)	16.855	0.747
Pan *et al*. (2021)	16.610	0.750
Ren *et al*. (2016)	19.068	0.765
Proposed	30.27549	0.93769

Table (3) shows a comparative analysis of PSNR and SSIM of the prevailing methods and the proposed method, where the proposed method has acquired a PSNR value of 30.27549 and SSIM of 0.93769.

Table (4) describes the PSNR acquired by the existing and the proposed model. Through Table (3) it is observed that the proposed model shows better results with 18.27.

From Table (5) it is observed that the proposed model is compared and achieved better results with a PSNR value of 30.27 and SSIM of 0.937 for the FRIDA dataset. Fig. (11) shows the comparison between the proposed and the FRIDA dataset and it is given below.

Table 4: Comparison of the FRIDA dataset with the proposed model (Wang *et al*., 2018)

Model	PSNR
He *et al*. (2010)	11.00000
Zhu *et al*. (2015)	10.20000
Existing	12.00000
Proposed	30.27549

Table 5: Comparative analysis of FRIDA dataset (Wang *et al*., 2018)

Model	PSNR	SSIM
Pan *et al*. (2021)	13.872	0.740
B2P+ADCP (Hartanto and Rahadianti, 2021)	15.276	0.751
MSCNN (Jiang *et al*., 2023)	16.437	0.830
Zhao *et al*. (2021)	18.373	0.917
Non-local (Zhang and He, 2020)	17.336	0.886
SDCP (Meng *et al*., 2022)	13.219	0.670
Tarel (Dong *et al*., 2020)	16.487	0.758
Meng *et al*. (2022)	15.404	0.821
Contrast (Ancuti *et al*., 2018)	12.385	0.69
Fattal (Tran *et al*., 2022)	13.232	0.816
Proposed	30.27549	0.93769

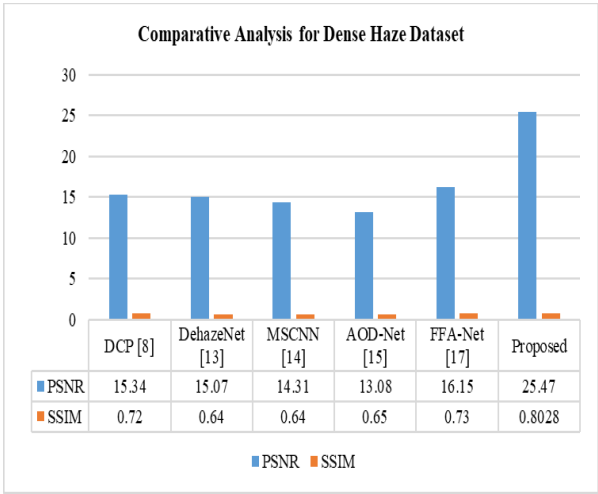

Fig. 10: Comparison of the proposed model with a conventional model for the dense haze dataset (Zhang and He, 2020)

Figure 10 it is inferred that the proposed model has attained greater results when compared with the existing model. Where it has attain PSNR value with 25.47 which is greater than the existing model. Similarly, the SSIM value is 0.8028 for the proposed model.

Figure (11) illustrates the comparison of results among the proposed and existing models for the FRIDA dataset. From the figure, it is inferred that the proposed model has obtained a PSNR value of 30.27. Moreover, for SSIM it has acquired 0.937. Hence it shows that the proposed model has attained greater results with the de-hazed images.

The proposed model reveals some advantages with certain limitations. A main advantage is its capacity to improve image sharpness and its features over the Focus Flex element that increases the visibility of things in hazy images. Furthermore, the Entropy Fade element particularly improves regions with less contrast by analyzing pixel intensity allocations, which causes a more regular de-hazing result. Moreover, the usage of an auto-encoder architecture permits for effective learning of the essential image structure, whereas the Intensity Attention System selects areas requiring further improvement, resulting in an advanced output. However, probable limitations comprise amplified computational complexity because of the combination of numerous components that may impact processing speed with real-world seemliness. Additionally, the efficacy of the mechanism in varied real-time situations relics to be confirmed, as the performance may differ reliant on the kinds of haze and image features encountered. Hence, the mechanism displays potential in refining de-hazing features, its real-world application may face encounters associated with efficacy and generality.

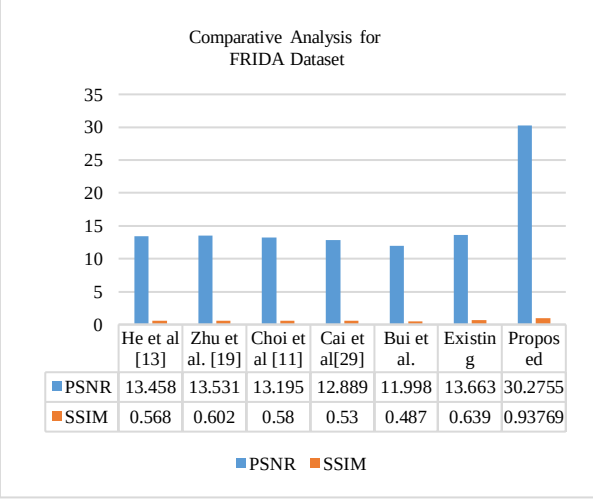

Fig. 11: Comparison of the proposed model with a conventional model for FRIDA dataset (Ren *et al*., 2016)

Conclusion

In the digital era, images hold an essential role where it representing individual ideas, experiences, and perceptive. Conversely, it is disturbed by various environmental circumstances. Specifically, hazed image is a substantial problem that affects the quality of the image. Since, manual de-hazing is time-consuming, prone to human error, and less efficacy, existing research used DL-based techniques for enhancing the de-hazing mechanism. However, it lacks in accuracy and speed. To tackle the problem, the presented system used Additionally, attention mechanism is used to highlight substantial data for enhancing the efficiency. Correspondingly, the performance of the proposed de-hazing method is evaluated with the performance metrics. The experimental results represent that the projected model attained of PSNR of 30.27549 and an SSIM value of 0.93769. Besides, the outcome of the comparative analysis signifies the greater efficiency of the proposed research. In the future, various image enhancement methods can be considered to improve the performance of the proposed research.

Acknowledgment

The author would like to thank an anonymous referee for giving very helpful comments and suggestions that have greatly improved this study.

Funding Information

The authors have not received any financial support or funding to report.

Author's Contributions

Rajat Tiwari: Original draft of the manuscript, written, methodology, revision and edited, conceptualization, submission.

Bhawna Goyal: Reviewed and edited, validation, supervision.

Ayush Dogra: Organization of manuscript, Revision methodology and edited.

Ethics

This article is original and contains unpublished material. The corresponding author confirms that all of the other authors have read and approved the manuscript and no ethical issues involved.

References

Ancuti, C. O., Ancuti, C., Timofte, R., & De Vleeschouwer, C. (2018). O-HAZE: A Dehazing Benchmark with Real Hazy and Haze-Free Outdoor Images. *2018 IEEE/CVF Conference on Computer Vision and Pattern Recognition Workshops (CVPRW)*, 867–8678. https://doi.org/10.1109/cvprw.2018.00119

Bi, G., Si, G., Zhao, Y., Qi, B., & Lv, H. (2022). Haze Removal for a Single Remote Sensing Image Using Low-Rank and Sparse Prior. *IEEE Transactions on Geoscience and Remote Sensing*, *60*, 1–13. https://doi.org/10.1109/tgrs.2021.3135975

Cimtay, Y. (2021). Smart and real-time image dehazing on mobile devices. *Journal of Real-Time Image Processing*, *18*(6), 2063–2072. https://doi.org/10.1007/s11554-021-01085-z

Dong, H., Pan, J., Xiang, L., Hu, Z., Zhang, X., Wang, F., & Yang, M.-H. (2020). Multi-Scale Boosted Dehazing Network with Dense Feature Fusion. *2020 IEEE/CVF Conference on Computer Vision and Pattern Recognition (CVPR)*, 2154–2164. https://doi.org/10.1109/cvpr42600.2020.00223

Hartanto, C. A., & Rahadianti, L. (2021). Single-Image Dehazing Based on Two-Stream Convolutional Neural Network. *JOIV : International Journal on Informatics Visualization*, *5*(1), 76–82. https://doi.org/10.30630/joiv.5.1.431

He, Y., Li, C., & Bai, T. (2023). Remote Sensing Image Haze Removal Based on Superpixel. *Remote Sensing*, *15*(19), 4680. https://doi.org/10.3390/rs15194680

He, K., Sun, J., & Tang, X. (2011). Single Image Haze Removal Using Dark Channel Prior. *IEEE Transactions on Pattern Analysis and Machine Intelligence*, *33*(12), 2341–2353. https://doi.org/10.1109/TPAMI.2010.168

Hovhannisyan, S. A., Gasparyan, H. A., Agaian, S. S., & Ghazaryan, A. (2022). AED-Net: A Single Image Dehazing. *IEEE Access*, *10*, 12465–12474. https://doi.org/10.1109/access.2022.3144402

Jiang, B., Wang, J., Wu, Y., Wang, S., Zhang, J., Chen, X., Li, Y., Li, X., & Wang, L. (2023). A Dehazing Method for Remote Sensing Image Under Nonuniform Hazy Weather Based on Deep Learning Network. *IEEE Transactions on Geoscience and Remote Sensing*, *61*, 1–17. https://doi.org/10.1109/tgrs.2023.3261545

Jiao, Q., Liu, M., Ning, B., Zhao, F., Dong, L., Kong, L., Hui, M., & Zhao, Y. (2022). Image Dehazing Based on Local and Non-Local Features. *Fractal and Fractional*, *6*(5), 262. https://doi.org/10.3390/fractalfract6050262

Meng, J., Li, Y., Liang, H., & Ma, Y. (2022). Single-Image Dehazing Based on Two-Stream Convolutional Neural Network. *Journal of Artificial Intelligence and Technology*, *2*(3), 100–110. https://doi.org/10.37965/jait.2022.0110

Mi, Z., Wang, Y., Zhao, C., Du, F., & Fu, X. (2020). Joint rain and atmospheric veil removal from single image. *IET Image Processing*, *14*(6), 1150–1156. https://doi.org/10.1049/iet-ipr.2019.0952

Meng, G., Wang, Y., Duan, J., Xiang, S., & Pan, C. (2013). Efficient Image Dehazing with Boundary Constraint and Contextual Regularization. *2013 IEEE International Conference on Computer Vision*. 2013 IEEE International Conference on Computer Vision (ICCV), Sydney, Australia. https://doi.org/10.1109/iccv.2013.82

Pan, J., Dong, J., Liu, Y., Zhang, J., Ren, J., Tang, J., Tai, Y.-W., & Yang, M.-H. (2021). Physics-Based Generative Adversarial Models for Image Restoration and Beyond. *IEEE Transactions on Pattern Analysis and Machine Intelligence*, *43*(7), 2449–2462. https://doi.org/10.1109/TPAMI.2020.2969348

Ren, W., Liu, S., Zhang, H., Pan, J., Cao, X., & Yang, M.-H. (2016). Single Image Dehazing via Multi-scale Convolutional Neural Networks. *Computer Vision -- ECCV 2016*, 154–169. https://doi.org/10.1007/978-3-319-46475-6_10

Roy, S. (2022). Single Image DnCNN Visibility Improvement (SImDnCNNVI). In *SSRN Electronic Journal*. https://doi.org/10.2139/ssrn.4139405

Tran, L.-A., Moon, S., & Park, D.-C. (2022). A novel encoder-decoder network with guided transmission map for single image dehazing. *Procedia Computer Science*, *204*, 682–689. https://doi.org/10.1016/j.procs.2022.08.082

Verma, M., Yadav, V., Kaushik, V. D., & Pathak, V. K. (2019). Multiple polynomial regression for solving atmospheric scattering model. *International Journal of Advanced Intelligence Paradigms*, *12*(3/4), 400–410. https://doi.org/10.1504/ijaip.2019.098604

Wang, K., Wang, H., Li, Y., Hu, Y., & Li, Y. (2018). Quantitative Performance Evaluation for Dehazing Algorithms on Synthetic Outdoor Hazy Images. *IEEE Access*, *6*, 20481–20496. https://doi.org/10.1109/access.2018.2822775

Wang, T., Zhao, L., Huang, P., Zhang, X., & Xu, J. (2021). Haze concentration adaptive network for image dehazing. *Neurocomputing*, *439*, 75–85. https://doi.org/10.1016/j.neucom.2021.01.042

Wu, Y., Qin, Y., Wang, Z., Ma, X., & Cao, Z. (2020). Densely pyramidal residual network for UAV-based railway images dehazing. *Neurocomputing*, *371*, 124–136. https://doi.org/10.1016/j.neucom.2019.06.076

Yang, C., Cao, F., Qi, D., He, Y., Ding, P., Yao, J., Jia, T., Sun, Z., & Zhang, S. (2020). Hyperspectrally Compressed Ultrafast Photography. *Physical Review Letters*, *124*(2), 023902. https://doi.org/10.1103/physrevlett.124.023902

Zhang, S., & He, F. (2020). DRCDN: learning deep residual convolutional dehazing networks. *The Visual Computer*, *36*(9), 1797–1808. https://doi.org/10.1007/s00371-019-01774-8

Zhao, W., Zhao, Y., Feng, L., & Tang, J. (2021). Attention Optimized Deep Generative Adversarial Network for Removing Uneven Dense Haze. *Symmetry*, *14*(1), 1. https://doi.org/10.3390/sym14010001

Zhu, Q., Mai, J., & Shao, L. (2015). A Fast Single Image Haze Removal Algorithm Using Color Attenuation Prior. *IEEE Transactions on Image Processing*, *24*(11), 3522–3533. https://doi.org/10.1109/tip.2015.2446191